Optimal Operation of Electrical and Thermal Resources in Microgrids with Energy Hubs Considering Uncertainties

Mohammad H. Shams [1], Majid Shahabi [1], Mohsen Kia [2], Alireza Heidari [3], Mohamed Lotfi [4], Miadreza Shafie-khah [5], and João P. S. Catalão [4,*]

[1] Department of Electrical and Computer Engineering, Babol Noshirvani University of Technology, Babol, Iran
[2] Department of Electrical Engineering, Faculty of Engineering, Pardis Branch, Islamic Azad University, Tehran, Iran,
[3] School of Electrical Engineering and Telecommunications, University of New South Wales (UNSW), Sydney, Australia
[4] Faculty of Engineering of the University of Porto (FEUP) and INESC TEC, 4200-465 Porto, Portugal
[5] School of Technology and Innovations, University of Vaasa, 65200 Vaasa, Finland

** corresponding author: catalao@fe.up.pt*

Abstract: Microgrids are often designed as energy systems that supply electrical and thermal loads with local resources such as combined heat and power units, renewable energy sources, diesel generators, and others. However, increasing interaction between natural gas and electrical systems, in addition to increased penetration of natural gas fired units gives rise to both opportunities and challenges in microgrid operation scheduling. In this paper, the energy hub concept is used to construct a scenario-based model for the optimal scheduling of electrical and thermal resources in a microgrid with integrated electrical and natural gas infrastructures. The objective function of the proposed model minimizes the expected operation costs while considering all network constraints and uncertainties. The natural gas and electricity flow equations are linearized and formulated as a mixed-integer linear programming problem. Scenarios associated with stochastic variables such as renewable generation and electrical and thermal loads are generated using the corresponding probability distribution functions and reduced using a scenario reduction technique. The proposed model is applied to an energy hub-based microgrid and the simulation results demonstrate the effectiveness of the approach. Furthermore, the benefits of implementing electrical and thermal demand response schemes are quantified. Also, more in-depth analyses for this network-constrained model are performed, including natural gas flow rate variations, natural gas pressures, power flow, and nodal voltages.

Keywords: Electrical-Thermal Scheduling, Microgrid, Energy Hub, Stochastic Programming.

List of Acronyms

CHP	Combined Heat and Power
DER	Distributed Energy Resources
DR	Demand Response
EH	Energy Hub
EMS	Energy Management System
FDM	Finite-Differences Method
GHV	Gross Heating Value
IC	Initial Conditions
MG	Microgrid
MGO	Microgrid Operator
MILP	Mixed Integer Linear Programming
NG	Natural Gas
OPF	Optimal Power Flow
PDF	Probability Distribution Function
PV	Photovoltaic
RES	Renewable Energy Sources
SOC	State of Charge

Nomenclature

	Indices
t	Time periods, t= 1, 2, …, T
i, j	Energy carriers nodes, i= 1, 2, …, I
n	CHPs, n= 1, 2, …, N
bo	Boilers, bo= 1, 2, …, BO
m	Diesel generators, m= 1, 2, …, M
hs	Heat storages, hs= 1, 2, …, H
b	Batteries, b= 1, 2, …, B
d	Responsive loads, d= 1, 2, …, D
s	Scenarios, s= 1, 2, …, S
wt	Wind turbines wt=1, 2, …, WT
pv	Photovoltaic systems pv=1, 2, …, PV
g	Natural Gas
e	Electricity
h	Heat
st	Steps of offered capacity by responsive loads
ch	Charge
dis	Discharge
U	Up-spinning reserve
D	Down-spinning reserve
max/min	Upper/lower limits
	Variables and parameters
S	Apparent power [kVA]
P	Power of energy carriers [kW]
Q	Reactive Power [kVar]
ES	Stored energy in heat storages [kWh]
SOC	State of charge in batteries [kWh]

V	Magnitude of voltage [p.u.]
δ	Voltage angel [rad]
Pr	Pressure of NG in pipelines [p.u.]
q	Offered capacity by responsive load [kW]
SUC	Start-up cost [$]
R	Scheduled reserve [kW]
EDR	Scheduled electrical demand response reserve [kWh]
TDR	Scheduled thermal demand response reserve [kWh]
r	Deployed reserve [kW]
edr	Deployed electrical demand response reserve [kW]
tdr	Deployed thermal demand response reserve [kW]
$EENS$	Electrical energy not supplied [kW]
$TENS$	Thermal energy not supplied [kW]
$f_d(l)$	Normal PDF for load l
$f_w(v)$	Rayleigh PDF for wind speed v
$f_b(r)$	Beta PDF for solar irradiance r
u	Indicates on/off (charge/discharge) status (1/0)
EL	Electric load [kW]
TL	Thermal load [kW]
η	Efficiency of components
K	Start-up cost constant [$]
G_{ij}	Real part of Y_{ij}, element in MG admittance matrix [p.u.]
B_{ij}	Imaginary part of Y_{ij}, element in MG admittance matrix [p.u.]
π	Prices [$]
$VoLL_e$	Value of loss of electrical load [$]
$VoLL_h$	Value of loss of thermal load [$]

1 Introduction

Local energy generation through electrical and thermal systems (e.g. using renewable energy sources (RES), combined heat and power (CHP), and diesel generation systems) has been causing an observable evolution in energy systems. The increased penetration of these distributed energy resources (DER) has resulted in more challenging tasks such as operation scheduling, cost and loss reductions, peak shaving, and demand side management. The microgrid (MG) concept was developed as a proposed solution to these newly emerging complex, albeit necessary, tasks in power systems. Meanwhile, the Energy Hub (EH) concept has also been attracting attention as a way to model energy conversion taking place through multiple integrated energy carries. An EH thereby interfaces different energy carriers (e.g. electricity, natural gas (NG), district heating) with the consumers, in which the input energy is converted and/or stored to be delivered through the desired carrier to the loads. EHs are made up of various elements, including transformers, boilers, heat storages, CHP, etc. [1] Therefore, operation scheduling of resources in an EH-based MG becomes highly complex with an increased number of EHs needed to supply the electrical and thermal loads. The complexity is further increased due to the presence of CHP in an EH, resulting in interdependence of electrical, thermal, and NG systems, and thereby making the operation scheduling of such a MG even more challenging task [2].

Numerous research works have investigated the different aspects of operation scheduling for MGs and energy systems in general. For optimal scheduling, the objective function generally accounts for fuel cost (local generation), reserve cost (local resources), and electricity prices (purchased from the grid) as shown in [3] and [4]. Additional levels of complexity (and accuracy) are achieved by accounting for: renewable generation uncertainties [5]; economic and environmental factors [6]; CHP coordination [7]; or storage and DR programs [8] in multi-objective two-stage stochastic MG scheduling, control, and energy management models. Meta-heuristic optimization approaches are commonly employed, such as in [9], where fixed and maintenance costs of battery storage systems were incorporated. A generalized risk-based stochastic modeling and scheduling framework considering wind integration in EH was proposed in [10].

So far, none of the mentioned studies accounted for the existence of a NG infrastructure. In general, there seems to be a need for more studies to consider the modeling, and resulting impacts thereof, of fully integrated NG infrastructures. There are indeed some researchers, which have addressed the interdependence of NG and electricity networks in operation scheduling. For instance, a mixed integer linear programming (MILP) formulation of optimal power flow (OPF) of the NG and electricity considering the security constraints is proposed in [11]. In this study, the effect of NG pipeline contingencies on the energy system operation is also considered. In [12], the growing need for NG-fired power plants and impact of NG prices on electricity markets was analyzed by using a security-constrained unit commitment approach. In [13], a stochastic day-ahead operation scheduling model is introduced using the management of up/down ramping of units to overcome the unpredictable

generation of renewable resources. In those previous studies, although the coupling of NG and electricity networks were considered, the coordinated operation scheduling of electrical and thermal loads are not addressed.

On a separate note, multiple studies on operation scheduling of interconnected EHs have recently been published. In [14], a method was developed to model and optimize systems with multiple-energy carriers and EHs. The first part of this paper addressed optimizing energy conversion in a single EH, as an economic dispatch between converters. The second part addressed optimal power flow in a system consists of several EHs. In [15], a bi-level linear model to determine the disruptive components and ensure resilient operation of coordinated electricity and NG infrastructures in an EH-based MG was proposed. In [16], a general unit commitment framework and a two-level hierarchical integrated control architecture for multiple energy carriers was proposed. It may be observed that the primary shortcoming of these aforementioned studies was ignoring the combination of various uncertainties in the scheduling and eliminating natural uncertainty of the problem. Therefore, the main improvements anticipated by the present study in comparison with previous literature of the authors are associated with identified shortcomings in the 1) objective function, 2) modeling of NG network, and 3) uncertainty modeling [17], [18].

In order to fill the research gaps identified in existing scientific literature, this study proposes an approach for optimal operation scheduling of EH-based MGs incorporating the following elements:

- A stochastic model for a multiple-energy carrier MG to supply thermal and electrical loads is proposed.
- Uncertainties of generation (wind and solar) and loads (electrical and thermal) are modeled by combining different scenarios.
- Taylor series is used to linearize the NG network equations, and a method is proposed to estimate initial NG pressures.
- DR programs are modeled and their effect on operation cost is analyzed.
- Security indices are imposed by adding constraints for limits on transmission line power, node voltage, and NG pressure.

The paper is organized as follows: Section 2 demonstrates the proposed EH-based MG model, its individual elements, the implemented DR program, in addition to the separate mathematical models for electrical and NG grids within the MG. Section 3 handles the stochastic problem formulation by considering different generation and load scenarios and combination thereof, leading to the formulation of the integrated MG model and the proposed operation scheduling optimization approach. Section 4 illustrates the case studies used to test the proposed model shows the results. Finally, Section 5, lists the corresponding conclusions of this study.

2 The MG Model

Figure 1 illustrates the proposed MG with a multiple-energy carrier infrastructure incorporating EHs, RES, battery storage, and a diesel generator. In this section, individual models for energy production, conversion, and transmission in the MG are described. This is followed by the mathematical modeling of the implemented DR program, and the separate models

for the electrical and NG grids. The uncertain behavior of the solar and wind generation and thermal and electrical loads is considered in the presented models by means of probability distribution functions (PDFs). Those are revisited in Section 3, when the integrated mathematical model is formulated, in order to generate scenarios for stochastic variables for the case studies.

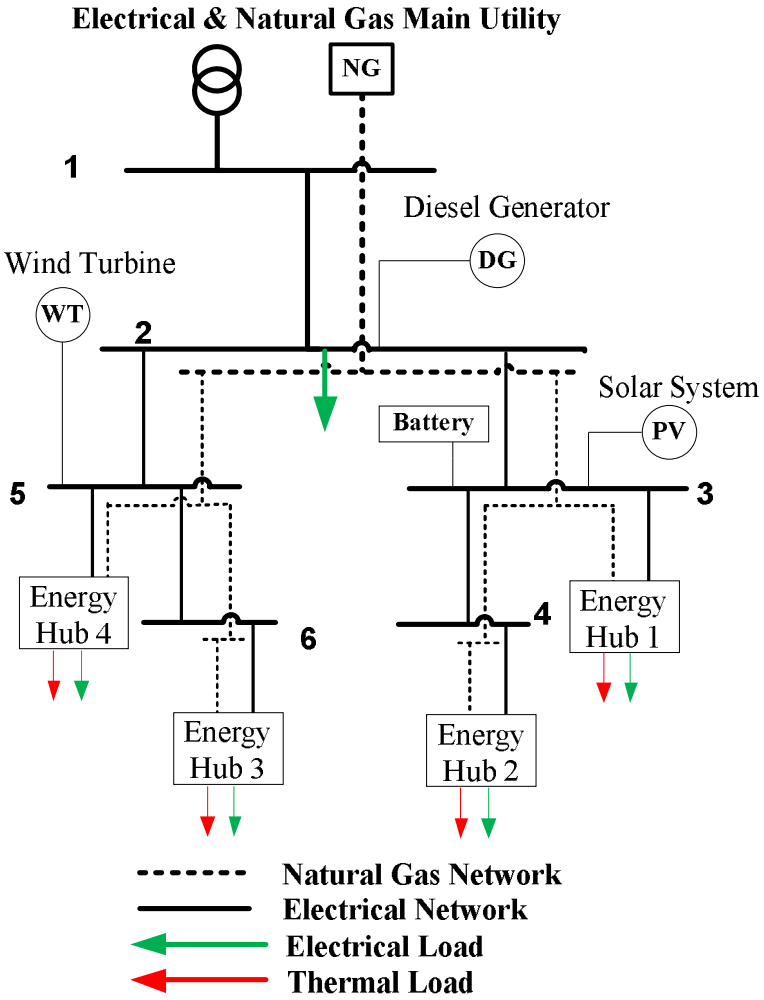

Figure 1: Schematic of the proposed EH-based multi-energy carrier MG.

2.1 Energy Hub

The coupling of an EH's inputs and outputs is depicted in Figure 2 and its corresponding mathematical representation in Eq. (1), where vectors L and P are output loads and input energy carriers, respectively. The EH coupling matrix C is associated with the efficiency values of the convertors. In this model, the EH elements are heat storage, boiler, transformer, and CHP. Those receive NG and electric power as input and supply thermal and electrical loads as output.

$$\underbrace{\begin{bmatrix} L_\alpha \\ \vdots \\ L_\omega \end{bmatrix}}_{L} = \underbrace{\begin{bmatrix} C_{\alpha\alpha} & \cdots & C_{\omega\alpha} \\ \vdots & \ddots & \vdots \\ C_{\alpha\omega} & \cdots & C_{\omega\omega} \end{bmatrix}}_{C} \underbrace{\begin{bmatrix} P_\alpha \\ \vdots \\ P_\omega \end{bmatrix}}_{P} \tag{1}$$

$$\alpha, \beta \in \varepsilon = \{ \text{electricity, NG, district heat, ...} \}$$

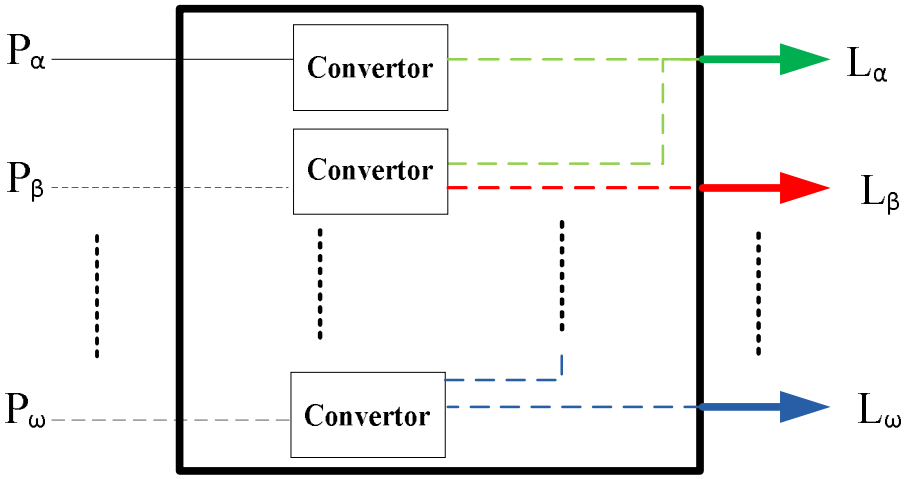

Figure 2: Depiction of input-output coupling in an EH through internal convertors.

2.2 Wind Turbine

Power generated by a wind turbine depends primarily on the incident wind speed. Atmospheric wind flow is always associated with turbulent components, which are chaotic by nature. Therefore, wind uncertainties are commonly modeled by means of statistical methods, such as using a Rayleigh PDF (derived from the Weibull distribution) to capture the wind behavior at a certain location. The Rayleigh (and Weibull) distribution was shown to provide a decent approximation for wind speed profiles. It is represented by Eq. (2), where c is a scale index equal to $\frac{2}{\sqrt{\pi}} \times v_{avg}$, and v_{avg} is the average incident wind speed at a particular location [19].

$$f_w(v) = \frac{k}{c}\left(\frac{v}{c}\right)^{k-1} \times \exp\left(-\left(\frac{v}{c}\right)^{k}\right) \tag{2}$$

Accordingly, piecewise linearization of the cubic power curve can be used to calculate a wind turbine's output power as a function of incident wind speed, as shown in Eq. (3). [20]

$$P_{wt,s}^{t} = \begin{cases} P_{wt,r} \quad , & v_r < v_s^t < v_{cout} \\ P_{wt,r}\dfrac{v_s^t - v_{cin}}{v_r - v_{cin}}, & v_{cin} < v_s^t < v_r \\ 0 \quad , & otherwise \end{cases} \tag{3}$$

P_{wt}^{t} is the output power at time t. $P_{wt,r}$ is the rated output of wind turbine (in kW). v_r, v_{cin}, v_{cout} are the rated wind speed, cut-in speed, and cut-out speed, respectively (m/s) [20].

2.3 Photovoltaic System

Photovoltaic (PV) systems convert sunlight into electric energy, in which the generated electrical power is a function of the amount of incident solar radiation on PV panels. Solar radiation can vary significantly due seasonal and meteorological changes, and thus the power generation of PV systems is associated with naturally high uncertainty. As was the case with wind generation, a statistical approach is often used to capture the stochastic behavior, with the Beta PDF commonly referenced as the best function to model the output power of PV cells [21]. This function is represented in Eq. (4).

$$f_b(r) = \begin{cases} \frac{\Gamma(\alpha+\beta)}{\Gamma(\alpha)\Gamma(\beta)} \mathrm{r}^{\alpha-1}(1-\mathrm{r})^{\beta-1}, 0 \le r \le 1, \alpha \ge 0, \beta \ge 0 \\ 0 \quad , \quad otherwise \end{cases} \tag{4}$$

The α and β parameters are represented in Eq. (5) in terms of the average (μ) and standard deviation (σ) of solar radiation for the period under study. The amount of incident solar radiation, r, is quantified in kW/m^2.

$$\beta = (1-\mu) \times \left(\frac{\mu \times (1+\mu)}{\sigma^2} - 1 \right), \alpha = \frac{\mu \times \beta}{1-\mu} \tag{5}$$

The output power of the solar photovoltaic system can be calculated by Eq.(6), using the efficiency of solar cells, the amount of incident solar radiation, and the collector (panels) surface area.

$$P_{pv,s}^t = \eta_{pv} . r_s^t . S_{pv} \tag{6}$$

P_{pv}^t is the output power of the photovoltaic system (in kW). η_{pv} and S_{pv} are the efficiency and the surface area of photovoltaic panels, respectively.

2.4 Thermal and Electrical Loads

It is important for the MG operator (MGO) to be capable of forecasting electrical and thermal demand for one-day-ahead (24 hours). The behavior of consumers, and thereby their energy demand, varies on different days and even throughout the hours of the day. The customers' demand is influenced by many factors such as weather conditions, social events, and official holidays, etc. Therefore, consumer demand is also modeled as stochastic variable and the uncertainty thereof is modeled by as a normal PDF, as expressed in Eq. (7), where μ and σ are the average and standard deviation of historical data of electrical and thermal loads, respectively [6].

$$f_d(l) = \left(\frac{1}{\sigma\sqrt{2\pi}} \right) \times \exp\left(-\frac{(l-\mu)^2}{2\sigma^2} \right) \tag{7}$$

2.5 Demand Response Program

In the proposed model for the MG scheduling, responsive electrical and thermal loads are anticipated. There are several models of DR programs in power system, such as incentive or price-based DR models, which encourage the participation of consumers. In the proposed MG model, it is assumed that all consumers have active energy management systems (EMS), which receive command signals such as the load reduction or curtailment requests from the MGO. In return, the EMS communicates back some data such as maximum participation in the load reduction program and the offered price to the MGO. The cost of electrical and thermal responsive loads ($CEDR_{d,s}^{t}$ and $CTDR_{d,s}^{t}$) are presented in Eq. (8), where $EDR_{d,s}^{t}$ and $TDR_{d,s}^{t}$ are the scheduled electrical and thermal demand response, respectively. $\pi_{e,d}^{t}$, $\pi_{h,d}^{t}$ are the corresponding offered prices, respectively

$$CEDR_{d,s}^{t} = EDR_{d,s}^{t} \times \pi_{e,d}^{t}$$
$$CTDR_{d,s}^{t} = TDR_{d,s}^{t} \times \pi_{h,d}^{t} \quad (8)$$

2.6 Electrical Grid

The power flow model in which neither voltage nor reactive power quantities are sacrificed, such as what is done in the DC model, nor does the number of equations increase like the line flow-based model is used based on reference [22]. Which is a good approximation since $(\delta_i^t - \delta_j^t)$ is usually small and voltage magnitudes are near 1 per unit. The active and reactive power injected to each node *i* at time *t*, as defined in Eq. (9) and Eq. (10). The electric power flow from node *i* to *j* at time *t* is represented in Eq. (11) and Eq. (12) [22], where P and Q are the active and reactive power flows, respectively. G and B are the real and imaginary components of the admittance matrix, respectively. Finally, V and δ are the magnitude and angle of nodal voltages, respectively.

$$P_{ei,s}^{t} = \sum_{j=1}^{J} (G_{ij}(V_{i,s}^{t} + V_{j,s}^{t} - 1) + B_{ij}(\delta_{i,s}^{t} - \delta_{j,s}^{t})) \quad (9)$$

$$Q_{ei,s}^{t} = \sum_{j=1}^{J} (-B_{ij}(V_{i,s}^{t} + V_{j,s}^{t} - 1) + G_{ij}(\delta_{i,s}^{t} - \delta_{j,s}^{t})) \quad (10)$$

$$P_{eij,s}^{t} = -G_{ij}(V_{i,s}^{t} - V_{j,s}^{t}) + B_{ij}(\delta_{i,s}^{t} - \delta_{j,s}^{t})) \quad (11)$$

$$Q_{eij,s}^{t} = B_{ij}(V_{i,s}^{t} - V_{j,s}^{t}) + G_{ij}(\delta_{i,s}^{t} - \delta_{j,s}^{t})) \quad (12)$$

2.7 Natural Gas Grid

The NG flow rate in the network lines depends on pipeline specifications, the pressure at both ends of each pipeline (boundary conditions), as well as fluid properties of the NG inside the pipelines. [23] This relationship is expressed by Eq. (13).

$$f_{ij,s}^{t} = k_{ij}\sqrt{\left|(Pr_{i,s}^{t})^2 - (Pr_{j,s}^{t})^2\right|} \tag{13}$$

$f_{ij,s}^{t}$ is the NG flow in the pipelines in m^3/day, $Pr_{i,s}^{t}$ is the NG pressure at node i, time t, and scenario s in kPa. k_{ij} is a variable representing the specifications of the pipeline connecting nodes i and j. Using Taylor series expansion, f_{ij}^{t} can be linearized using the backward finite differences method (FDM), to obtain the form shown in Eq. (14).

$$f_{ij,s}^{t} = k_{ij} \times \frac{(Pr_{i,s}^{t} \times Pr_{i}' - Pr_{j,s}^{t} \times Pr_{j}')}{\sqrt{\left|(Pr_{i}')^2 - (Pr_{j}')^2\right|}} \tag{14}$$

Pr_{i}' is the initial pressure at node i. The main challenge of using this linearization method is the need to set initial conditions (IC) which are as accurate as possible due to the sensitivity of the numerical method to them. Choosing IC will result in the divergence of the numerical approximation, leading to a wrong flow rate dispatch and a far from optimal answer. In the Appendix, the method used in this study to determine the IC is described with an illustrative example. To convert the NG flow through the pipelines to power flow, Gross Heating Value (GHV) can be used as shown in Eq. (15):

$$P_{g,ij,s}^{t} = GHV.f_{ij,s}^{t} \tag{15}$$

$P_{g,ij,s}^{t}$ is the NG power flow through a pipeline between nodes i and j, expressed in kW [14]. The NG balance at each node and time instant is represented in Eq. (16). The injected NG to a node i, $P_{gi,s}^{t}$, consists of consumed NG by the CHP and the boiler. The scheduled NG to purchase $P_{g,net,s}^{t}$ is determined by Eq. (17).

$$P_{gi,s}^{t} - \sum_{j=1}^{J_i} P_{g,ij,s}^{t} = 0\,, P_{gi,s}^{t} = P_{gi,s}^{t,chp} + P_{gi,s}^{t,bo} \tag{16}$$

$$P_{g,net,s}^{t} = \sum_{i=1}^{I} P_{gi,s}^{t} \tag{17}$$

3 Problem Formulation

In this problem, the objective is to construct a decision-making model to determine the optimal values for purchased electricity and NG from the energy market, commitment and output power of energy units, responsive loads, and involuntary load curtailments. To model real-life conditions of energy systems and markets, stochastic programming is employed to account for uncertainties by considering multiple scenarios. With this being an optimization problem, an objective function and constraints need to be mathematically defined, which is elaborated in detail in the subsequent sections.

3.1 Objective Function

The optimization problem at hand aims at solving for the right set of conditions to minimize the total costs of the system. Thus, the minimization function contains a summation of all costs associated with all scenarios and is shown in Eq. (18).

$$Minimize \sum_{s=1}^{S} \rho_s \left(\sum_{t=1}^{T} \left\{ P_{e,net,s}^{t}.\pi_e^t + P_{g,net,s}^{t}.\pi_g^t + \sum_{m=1}^{M} SUC_{m,s}^{t} + \sum_{n=1}^{N} SUC_{n,s}^{t} + \sum_{bo=1}^{BO} SUC_{bo,s}^{t} + \sum_{m=1}^{M} [C_{m,s}^{t}] \right. \right. \\ \left. \left. + \sum_{d=1}^{D} [CEDR_{d,s}^{t} + CTDR_{d,s}^{t}] + \sum_{i}^{I} [VoLL_e^t.EENS_{i,s}^{t} + VoLL_h^t.TENS_{i,s}^{t}] \right\} \right) \quad (18)$$

ρ_s is the probability of scenario *s*. The rows/terms in the summation (for each scenario) correspond to: cost of scheduled purchased electricity and NG from the main grid, start-up cost of units ($SUC_{\bullet,s}^{t}$), fuel cost of diesel generators ($C_{m,s}^{t}$), the cost of reduced electrical and thermal demand, and the cost of involuntary thermal and electrical load curtailments (where $VoLL$ is value of loss of electrical/thermal load). Finally, $EENS$ and $TENS$ are electrical and thermal energy, respectively, which is not supplied in the case of load curtailments.

3.2 Constraints

After defining the objective function, the next step is to define the physical and numerical constraints for which limit the feasible solution domain. The constraints used in this model are listed in Eq. (19)-(42), which are elaborated in detail below.

Eq. (19) is a conservation equation that describes the balance of total electrical energy. The RHS of Eq. (19) is expanded in Eq. (20) accounting for the efficiency of CHP. Similarly, Eq. (21)-(23) present the thermal energy balance. The start-up cost of units by Eq. (24)-(26). The binary variable (u) is used to indicate the on/off status of resources. The limitation of the thermal and electrical output power of units is represented by Eq. (27) and Eq. (28), respectively. In Eq. (29), quantity of heat energy stored is described and Eq. (30) guarantees that heat energy storage is always either charging or discharging. Eq. (31) limits the minimum and maximum discharge and charge power of the heat storage. The cost of diesel generators is represented by Eq. (32) and their minimum and maximum power output is limited by Eq. (33). In Eq. (34), the state of charge (SOC) of the battery

is represented. As with thermal storage, Eq. (35) guarantees the battery is always either charging or discharging by means of the binary variable *u*, which is then imposed in Eq. (36). Eq. (37) imposes the restriction that the scheduled capacity of thermal and electrical load reduction for any responsive load should be less than or equal to its maximum offered capacity. The limitation of scheduled electricity to purchase from the main grid is set by Eq. (38). The security constraints of the electricity network are considered by Eq. (39). In Eq. (40), the limitation of scheduled NG purchase is determined. In addition, the NG network security constraints are incorporated by means of the maximum power flow in pipelines and NG pressure at nodes, as shown in Eq. (41). The amount of involuntary electrical and thermal load curtailment is a non-negative variable with a limitation described in Eq. (42).

$$\sum_{n=1}^{N_i} P_{e,n,s}^{t} + \sum_{m=1}^{M_i} P_{m,s}^{t} + \sum_{wt=1}^{WT_i} P_{wt,s}^{t} + \sum_{pv=1}^{PV_i} P_{pv,s}^{t} + \sum_{b=1}^{B_i} \left(P_{b,s}^{t,dis} - P_{b,s}^{t,ch}\right) + \sum_{d=1}^{D_i} EDR_{d,s}^{t} - EL_{i,s}^{t} + EENS_{i,s}^{t} = P_{ei,s}^{t} \tag{19}$$

$$P_{e,n,s}^{t} = \eta_{CHP,e} \times P_{gi,s}^{t,CHP} \tag{20}$$

$$\sum_{n=1}^{N_i} P_{h,n,s}^{t} + \sum_{bo}^{Bo_i} P_{bo,s}^{t} + \sum_{hs=1}^{HS_i} \left(P_{hs,s}^{t,dis} - P_{hs,s}^{t,ch}\right) + \sum_{d=1}^{D_i} TDR_{d,s}^{t} + TENS_{i,s}^{t} = TL_{i,s}^{t} \tag{21}$$

$$P_{bo,s}^{t} = \eta_{Bo} \times P_{gi,s}^{t,bo} \tag{22}$$

$$P_{h,n,s}^{t} = \eta_{CHP,h} \times P_{gi,s}^{t,CHP} \tag{23}$$

$$SUC_{m,s}^{t} \geq 0, SUC_{m,s}^{t} \geq K_m \times (u_{m,s}^{t} - u_{m,s}^{t-1}) \tag{24}$$

$$SUC_{n,s}^{t} \geq 0\ , SUC_{n,s}^{t} \geq K_n \times (u_{n,s}^{t} - u_{n,s}^{t-1}) \tag{25}$$

$$SUC_{bo,s}^{t} \geq 0\ , SUC_{bo,s}^{t} \geq K_{bo} \times (u_{bo,s}^{t} - u_{bo,s}^{t-1}) \tag{26}$$

$$\begin{gathered} P_{e,n}^{min} \times u_{n,s}^{t} \leq P_{e,n,s}^{t} \leq P_{e,n}^{max} \times u_{n,s}^{t} \\ P_{h,n}^{min} \times u_{n,s}^{t} \leq P_{h,n,s}^{t} \leq P_{h,n}^{max} \times u_{n,s}^{t} \end{gathered} \tag{27}$$

$$P_{bo}^{min} \times u_{bo,s}^{t} \leq P_{bo,s}^{t} \leq P_{bo}^{max} \times u_{bo,s}^{t} \tag{28}$$

$$\begin{gathered} ES_{hs,s}^{t} = ES_{hs,s}^{t-1} + \eta_{hs}^{ch} \times P_{hs,s}^{t,ch} - 1/\eta_{hs}^{dis} \times P_{hs,s}^{t,dis} - E_{hs} \\ ES_{hs}^{min} \leq ES_{hs,s}^{t} \leq ES_{hs}^{max} \end{gathered} \tag{29}$$

$$u_{hs,s}^{t,ch} + u_{hs,s}^{t,dis} \leq 1 \tag{30}$$

$$\begin{gathered} 0 \leq P_{hs,s}^{t,ch} \leq P_{hs}^{ch,max} \times u_{hs,s}^{t,ch} \\ 0 \leq P_{hs,s}^{t,dis} \leq P_{hs}^{dis,max} \times u_{hs,s}^{t,dis} \end{gathered} \tag{31}$$

$$C_{m,s}^{t} = a_m \times u_{m,s}^{t} + b_m \times P_{m,s}^{t} \tag{32}$$

$$P_m^{min} \times u_{m,s}^{t} \leq P_{m,s}^{t} \leq P_m^{max} \times u_{m,s}^{t} \tag{33}$$

$$\begin{gathered} SOC_{b,s}^{t} = SOC_{b,s}^{t-1} + \eta_b^{ch} \times P_{b,s}^{t,ch} - 1/\eta_b^{dis} \times P_{b,s}^{t,dis} \\ SOC_b^{min} \leq SOC_{b,s}^{t} \leq SOC_b^{max} \end{gathered} \tag{34}$$

$$u_{b,s}^{t,ch} + u_{b,s}^{t,dis} \leq 1 \tag{35}$$

$$\begin{gathered} P_{b,s}^{t,ch} \leq P_b^{ch,max} \times u_{b,s}^{t,ch} \\ P_{b,s}^{t,dis} \leq P_b^{dis,max} \times u_{b,s}^{t,dis} \end{gathered} \tag{36}$$

$$\begin{gathered} 0 \leq EDR_{d,s}^{t} \leq EDR_d^{t,max} \\ 0 \leq TDR_{d,s}^{t} \leq TDR_d^{t,max} \end{gathered} \tag{37}$$

$$P_{e,net}^{min} \leq P_{e,net,s}^{t} \leq P_{e,net}^{max} \tag{38}$$

$$\left|S_{eij,s}^{t}\right| \leq S_{eij}^{max}, \qquad V_i^{min} \leq V_{i,s}^{t} \leq V_i^{max} \tag{39}$$

$$0 \leq P_{g,net,s}^{t} \leq P_{g,net}^{max} \tag{40}$$

$$\left|P_{g,ij,s}^{t}\right| \leq P_{g,ij}^{max}, \quad Pr_i^{min} \leq Pr_{i,s}^{t} \leq Pr_i^{max} \tag{41}$$

$$EENS_{i,s}^{t} \leq EL_{i,s}^{t}, TENS_{i,s}^{t} \leq TL_{i,s}^{t} \tag{42}$$

3.3 Scenario Generation and Reduction Method

After defining the objective function and all problem constraints, the final step is to generate the scenarios required for a stochastic optimization model, which model the various natural uncertainties present in the system.

To generate scenarios for wind and PV generation, in addition to load uncertainty, the PDFs described in Section 2 were utilized in order to be incorporated into the model. Figure 3 illustrates the algorithm used to obtain the best scenarios and their associated probabilities. As shown in this figure, MATLAB functions are used to generate PDF-based random variables. Afterwards, the vector of scenarios for all times ($X(s,t) = [EL_s^t, TL_s^t, P_{wt,s}^t, P_{pv,s}^t]$) is presented with probability of 1/NS.

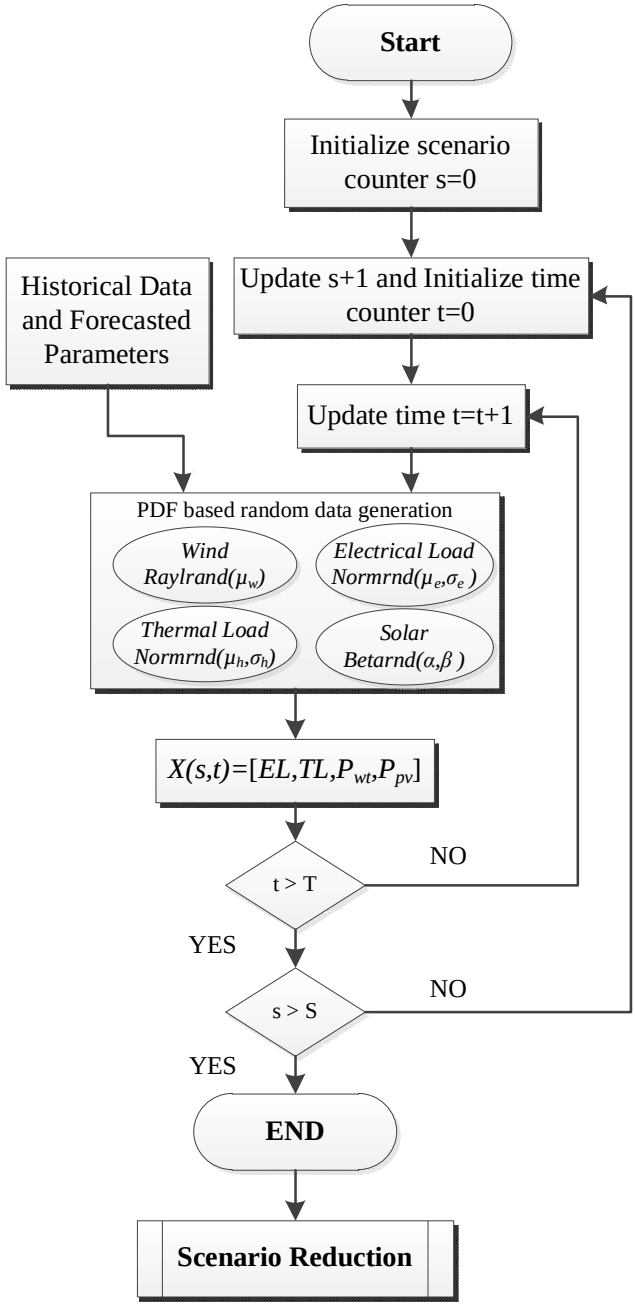

Figure 3: Flowchart of scenario generation and reduction approach

After obtaining the full set of scenarios, their number is reduced in order to leverage the computational efficiency of the model. This was performed using the Forward Method in SCENRED tool, which is part of the GAMS software package [24].

The reduction algorithms developed in SCENRED determine a subset of the initial scenario set and assign new probabilities to the preserved scenarios. All deleted scenarios have probability zero. The reduction algorithms exploit a certain probability distance of the original and the reduced probability measure. The probability distance trades off scenario probabilities and distances of scenario values. Therefore, deletion will occur if scenarios are close or have small probabilities.

Using this method 100 scenarios are generated and consequently based on the results accuracy, the number of the reduced scenarios are obtained to 3. It should be mentioned that the more scenarios is results in more accuracy.

4 Case Studies

4.1 Data

The proposed model is applied to the 6-node EH-based MG illustrated in Figure 1. For this MG, the hourly electrical load and price, thermal load, and NH price are shown for a 24-hour period in Figure 4-(a). The hourly wind speed and solar irradiance values for the same period are shown Figure 4-(b). Electrical and thermal load ratios at the network nodes are shown in Table 1. Table 2 lists the offered capacity and the price of responsive electrical and thermal loads. Specification of NG pipelines and electrical lines are described in Table 3.

Table 1: Load ratios in different nodes

Node No.	**1**	**2**	**3**	**4**	**5**	**6**
Heat Load	-	-	0.47	0.25	0.14	0.14
Active Load	-	0.11	0.45	0.22	0.11	0.11
Reactive Load	-	0.03	0.15	0.07	0.03	0.03

Table 2: Offered capacity and price by responsive loads

T	$EDR_d^{t,max}$ kW	$\pi_{e,d}^t$ $Cent/kWh$	$TDR_d^{t,max}$ kW	$\pi_{h,d}^t$ $Cent/kWh$
1	13	3	104	5
2	12	3	97	5
3	16	3	94	5
4	17	4	87	5
5	22	3	84	5
6	41	3	81	5
7	61	3	84	5
8	74	5	85	5

T	$EDR_d^{t,max}$ kW	$\pi_{e,d}^t$ $Cent/kWh$	$TDR_d^{t,max}$ kW	$\pi_{h,d}^t$ $Cent/kWh$
9	77	5	84	4
10	81	14	75	4
11	77	13	61	4
12	79	10	65	4
13	71	3	74	4
14	73	3	75	4
15	72	3	77	4
16	73	3	71	4
17	76	3	81	4
18	83	6	82	4
19	84	6	87	5
20	83	7	91	5
21	78	7	91	5
22	58	5	100	5
23	55	4	110	5
24	41	3	100	5

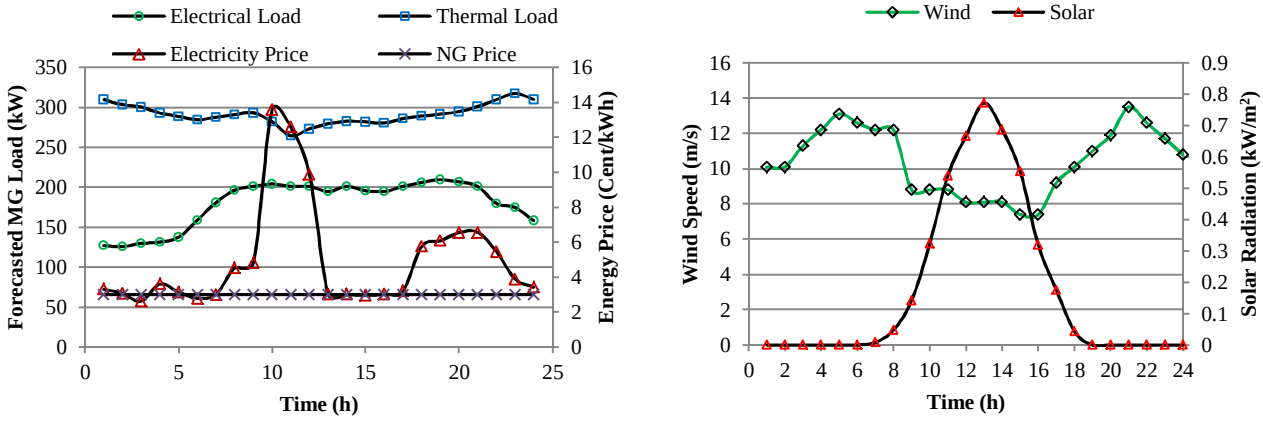

(a) (b)

Figure 4: Forecasted day-ahead (a) load profile and energy price, (b) solar irradiance and wind speed.

Table 3: Characteristics of electrical lines and NG pipelines

Electrical Network			**NG Network**	
Line	R_{ij}	X_{ij}	Line	$GHV \times K_{ij}$
1-2	0.01335	0.04211	-	-
2-3	0.01938	0.05917	2-3	8
3-4	0.0312	0.16	3-4	13
2-5	0.0228	0.12	2-5	9
5-6	0.0228	0.12	5-6	9

The specifications of various EH elements and resources in the MG are described in Tables 4 and 5, respectively. The charge and discharge efficiency for heat storage and the battery were set to 0.9. The limits of power and NG flow through lines are 1 per unit. The permissible range of NG pressure and voltage magnitude at nodes is considered between 0.9 - 1.1 and 0.95-1.05 per unit, respectively.

Table 4: Specifications of CHP, Heat Storage, Boiler, and Transformer in the MG under study.

CHP		**Heat Storage**		**Boiler**	
$\eta_{CHP,e}$	0.42	η_h^{ch}	0.9	K_{Bo}	15
$P_{CHP,e}^{min}$	4	η_h^{dis}	1	η_{Bo}	0.85
$P_{CHP,e}^{max}$	33	ES_h^{min}	0	P_{Bo}^{min}	0
$\eta_{CHP,h}$	0.47	ES_h^{max}	33	P_{Bo}^{max}	110
$P_{CHP,h}^{min}$	5	$P_{h,max}^{ch}$	6	**Transformer**	
$P_{CHP,h}^{max}$	55	$P_{h,max}^{dis}$	16	1	η_T
K_n	15				

Table 5: Specifications of Battery, Diesel Generator, Wind Turbine, and PV in the MG under study

Battery		**Diesel Generator**		**Wind Turbine**	
η_b^{ch}	0.9	K_m	15	$P_{wt,r}$	24
η_b^{dis}	0.9	a_m	50	v_{cin}	3
SOC_b^{min}	0	b_m	5.3	v_{cout}	50
SOC_b^{max}	54	c_m	0.1	v_r	12
$P_{b,max}^{ch}$	36	$P_{DG,m}^{min}$	3	**Photovoltaic**	
$P_{b,max}^{dis}$	36	$P_{DG,m}^{max}$	30	η_{pv}	0.186
				S_{pv}	64

4.2 Results and Discussion

The proposed model is a mixed integer linear programming (MILP) problem which was implemented using the GAMS package [25]. To scrutinize the effectiveness of the proposed approach for modern MGs, two different case studies were devised:

- Case Study 1: Proposed stochastic scheduling model without DR programs.
- Case Study 2: Proposed stochastic scheduling model with DR programs.

In both case studies, 100 scenarios were generated for each time increment. Each scenario has a probability of 0.01 and consists of four stochastic variables (thermal and electrical loads of MG, solar irradiation and, wind speed). Using the SCENRED tool in GAMS software environment, the scenarios are reduced to 3 best representative scenarios. Table 6 illustrates the reduced scenarios and their probability in comparison with the forecasted values for *t=14.*

Table 6: Comparison of uncertain variables in scenarios at t=14

Scenario No.	**1**	**2**	**3**	**Forecasted**
Electrical Load (kW)	180.6	206.4	154.8	172
Thermal Load (kW)	264.1	250.2	333.6	278
Wind Speed (m/s)	7.2	8.2	9.2	8.1
Solar irradiation (kW/m^2)	0.65	0.67	0.57	0.68
Probability	0.598	0.248	0.154	1

As shown in Table 7, Case 2 (with DR implementation) has a significantly lower total operation cost compared to Case 1 (without DR implementation). The 15% decrease in total operation cost and the tenfold decrease in curtailed load come to show the significant economic and operational impact of DR program implementation.

Table 7: Operation costs in cases 1 and 2

Case No.	Energy Cost($)	DR Cost($)		Expected Curtailed Load Cost ($)	Total Expected Operation Cost($)
		Elc.	Thrl.		
1	394.61	-	-	77.89	472.5
2	376.52	6.29	10.33	7.91	401.05

A more in-depth analysis is now presented based on Case 2, Scenario 1. Figure 5 and Figure 6 demonstrate the optimal scheduling of electrical and thermal power in the 24-hour day-ahead horizon. In Figure 5, it can be seen that higher CHP and diesel power generation are present during hours with high electricity prices (i.e. 10:00 to 12:00 and 18:00 to 22:00), which also corresponds to minimum purchased electricity from the grid is at the minimum. Furthermore, the battery is charged at low prices and low demand (i.e. at 3:00, 6:00, and 13:00 to 15:00) and discharged in high rates or peak loads such (i.e. 9 :00 to 12:00). The RESs power generation can be confirmed to be in accordance with the forecasted parameters.

Similarly, Figure 6 shows the thermal energy scheduling results. Most of the energy is provided by the boilers due to their high efficiency and capacity. It is shown that heat storage is charged during hours of low demand and discharged during those

of peak load. In these figures the dashed lines are the modified load profiles by utilizing responsive loads offers. As a result of the limited capacity of the natural gas pipelines, the thermal energy cannot be fully supplied by boilers that utilize natural gas. Therefore, the heat storage facilities are scheduled to provide thermal energy to the consumers at such periods. As shown in these figures, the price of electricity affects the schedule of electricity and thermal energy supply in the microgrid.

The results of electricity and NG power flow at the critical points are shown in Table 8. The node and time of the minimum and maximum of the NG pressure, voltage magnitude, as well as energy flows are listed in this table. Figure 7-(a) depicts the NG pressures at pipeline nodes. Since the NG network is radial, the downstream nodes of pipelines have less pressure than the upstream ones. Intuitively, the nodes with higher demand have less pressure than the others since NG flows downstream of the pressure gradient. As a result, nodes 3 and 4 have the least NG pressure in this MG. Figure 7-(b) shows the voltage magnitude of MG nodes. Node 4 has the lowest voltage because of their location at the end of the feeders and the load ratios on this feeder.

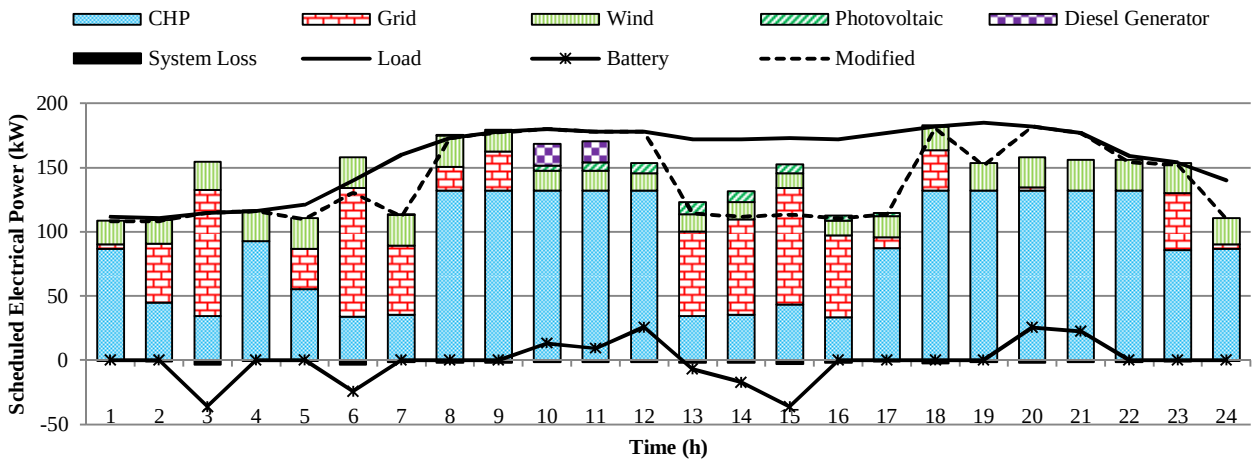

Figure 5: Day-ahead schedule for electrical power.

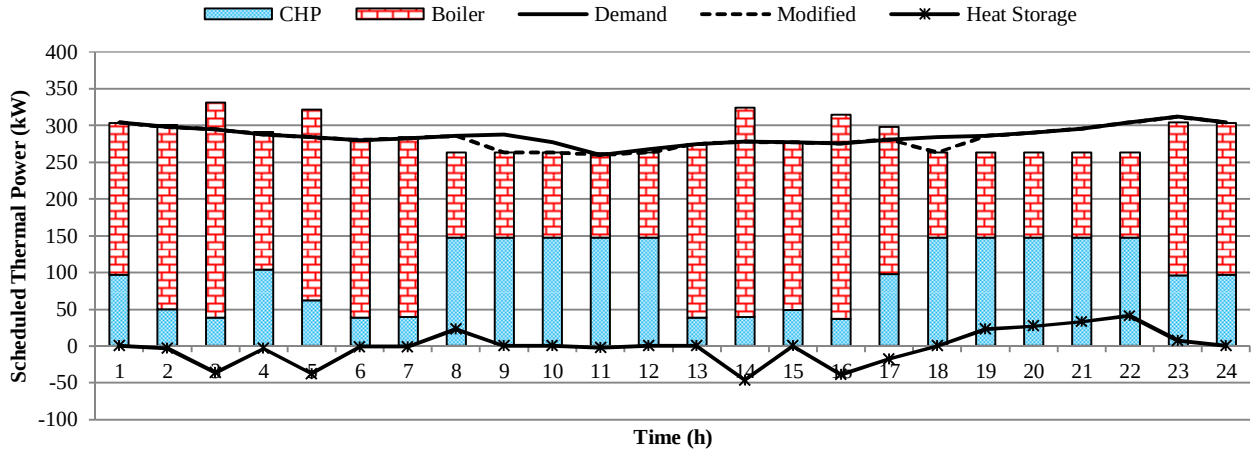

Figure 6: Day-ahead schedule for thermal power.

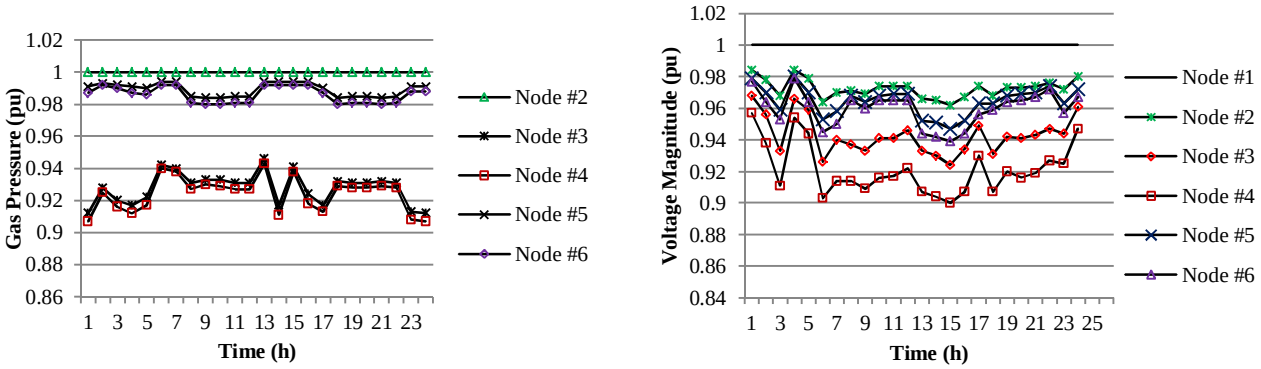

(a) (b)

Figure 7: Optimal energy flow results at the nodes for: (a) NG pressure, and (b) Voltage magnitude

Table 8: Power flow results in critical points

Case No.	Min. NG Pressure (pu)	Min. Voltage (pu)	Max. Active Power Flow (kW)	Max.NG Flow (kW)
	Node, Time	Node, Time	Node, Time	Node, Time
1	0.903 i4 at t23	0.9 i4 at t15	100 i1 to i2 at t3, t6	434.53 i2 to i3 at t1
2	0.907 i4 at t1, t24.	0.9 i4 at t15	100 i1 to i2 at t6	427.76 i2 to i3 at t1

Finally, Figure 8 shows that by reducing the NG pipelines capacity, the NG network is congested and consequently the expected operation cost exponentially increases. However, increasing the capacity beyond 42 m^3/h is met with a convergence of the expected operation cost to around 395$. I.e., increasing the capacity beyond this point does not result in any reduction of costs due to the limitations of components' capacity. Thereby, the NG network constraints have a significant, direct, effect on both the operation scheduling and operation costs.

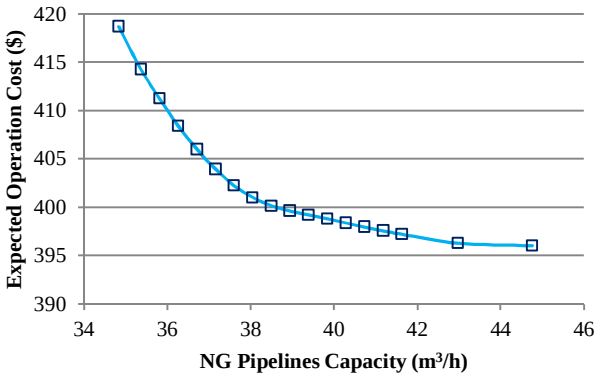

Figure 8: Sensitivity analysis: expected cost versus the NG pipelines capacity.

5 Conclusions

In this paper, an efficient stochastic model for energy scheduling of an energy hub-based microgrid was proposed, integrating the models for electrical, thermal and natural gas infrastructures. In this model, the uncertainties associated with both generation (wind and photovoltaic) and load in the microgrid were considered and modeled using their corresponding probability distribution functions. The complex natural gas flow equations were linearized using a robust approximation, in order to include them in the integrated MILP optimization model. The constraints associated with the electrical and natural gas networks were applied to the model to evaluate the interdependence of these networks. The proposed model was implemented using GAMS and tested on a 6-bus microgrid with 4 energy hubs with electrical, thermal, and natural gas infrastructures, in addition to both electrical and thermal storage capabilities, in order to analyze its performance. The results demonstrated the effectiveness of the proposed approach and it was shown through further analysis that implementing electrical and thermal demand response programs plays an essential role in significantly reducing the curtailed loads (tenfold) as well as the operation costs (15%). Furthermore, following the economic dispatch in both electrical and natural gas networks, the critical nodes, pipelines, and feeders were identified. Finally, a sensitivity analysis revealed that total operation costs were increased significantly with small decreases in natural gas capacities, such as those caused by congestions in the pipelines. Meanwhile, there exists a threshold for pipeline capacity, beyond which there is no added economic benefit. The proposed scheduling tool, as well as the above-mentioned analysis of the case studies, can be very useful for a microgrid operator to operate and control a multiple-energy carrier microgrid. The future of this work can be established on resilient oriented operation of energy hub-based microgrids. Also, facing with the nonlinear equations as well as uncertainties can be considered in future works.

Appendix – Calculating the Initial Conditions for the NG Flow Model

It was mentioned in Section 2.7 that the linearization of the NG flow equations using the backward-FDM (with the Taylor series expansion) requires an accurate approximation of the IC as the formulation is very sensitive to them. In this appendix the method used to approximate the IC (initial NG pressure values at *t=1*) is demonstrated.

To determine the initial pressure of the NG network, consider a 4-node NG network such as the one shown in Figure A-1, as a simplified example to describe the proposed method. Equation A-1 represents the flow rate of NG in pipelines.

$$[f] = [A].\left[\frac{TL}{\eta}\right] = k_{ij}\sqrt{\left|(Pr_i)^2 - \left(Pr_j\right)^2\right|} \tag{A-1}$$

Where $[A]$ is the network matrix, which determines the flow direction within the network. The elements, a_{ij} are equal to 1 if node *i* is located upstream of node *j*, and zero otherwise. The other matrix, $[TL/\eta]$ represents the consumed NG by a thermal load at node *i*.

As a demonstration of how the matrices can be constructed, consider that the thermal loads at nodes 3 and 4 are 1.1, and 1.2 pu, respectively. Also, the coefficients $GHV \times K_{ij}$ for pipelines between nodes 1-2, 2-3, and 2-4 are 9, 7, and 6, respectively. The efficiency of CHPs and/or boilers is assumed to be 0.5.

Moreover, the pressure at node 1 is considered to be equal to 1 p.u., as the reference node to normalize the rest of the values As such, the matrices can be evaluated using Eq. (A-2) and (A-3), and the corresponding values of pressure can be obtained as shown in Eq. (A-4) to (A-6).

$$\underbrace{\begin{bmatrix} f_{12} \\ \vdots \\ f_{ij} \end{bmatrix}}_{f} = \underbrace{\begin{bmatrix} a_{11} & \cdots & a_{1j} \\ \vdots & \ddots & \vdots \\ a_{i1} & \cdots & a_{ij} \end{bmatrix}}_{A} \underbrace{\begin{bmatrix} TL_1/\eta_1 \\ \vdots \\ TL_i/\eta_i \end{bmatrix}}_{TL/\eta} \tag{A-2}$$

$$\begin{bmatrix} f_{12} \\ f_{23} \\ f_{24} \end{bmatrix} = \begin{bmatrix} 0\ 1\ 1\ 1 \\ 0\ 0\ 1\ 0 \\ 0\ 0\ 0\ 1 \end{bmatrix} \begin{bmatrix} 0 \\ 0 \\ 1.1/0.5 \\ 1.2/0.5 \end{bmatrix} \tag{A-3}$$

$$f_{12} = 4.6 = 9.\sqrt{|(1)^2 - (Pr_2)^2|} \Rightarrow Pr_2 = 0.85\ p.u \tag{A-4}$$

Consequently, Pr_3 and Pr_4 will be:

$$f_{23} = 2.2 = 7.\sqrt{|(0.85)^2 - (Pr_3)^2|}$$

$$\Rightarrow Pr_3 = 0.79\ p.u \tag{A-5}$$

$$f_{24} = 2.4 = 6.\sqrt{|(0.85)^2 - (Pr_4)^2|}$$

$$\Rightarrow Pr_4 = 0.75\ p.u \tag{A-6}$$

The above-described method was applied to the case study of this paper in order to determine the initial node presses. As such, these values are used as the IC of the linearized model for the NG flow equations.

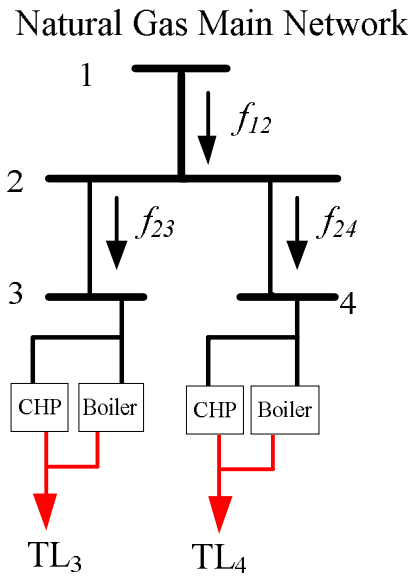

Figure A-1: Example of radial NG network.

Acknowledgment

J.P.S. Catalão acknowledges the support by FEDER funds through COMPETE 2020 and by Portuguese funds through FCT, under POCI-01-0145-FEDER-029803 (02/SAICT/2017). Also, M. Lotfi would like to acknowledge the support of the MIT Portugal Program (in Sustainable Energy Systems) by Portuguese funds through FCT, under grant PD/BD/142810/2018.

References

[1] M. Geidl, G. Koeppel, P. Favre-Perrod, B. Klockl, G. Andersson, K. Frohlich, “The energy hub – a powerful concept for future energy systems,” The third annual Carnegie Mellon conference on the electricity industry; March 2007.

[2] Gu, Wei, et al. “Modeling, planning and optimal energy management of combined cooling, heating and power microgrid: A review,” International Journal of Electrical Power & Energy Systems, vol. 54, pp. 26-37, 2014.

[3] C. Chen, S. Duan, T. Cai, “Smart energy management system for optimal microgrid economic operation,” IET Renewable power generation, vol. 5, pp.258-267, 2011.

[4] A. G. Tsikalakis, N. D. Hatziargyriou, “Centralized control for optimizing microgrids operation,” IEEE Trans. Energy Convers., vol. 23, pp. 241–248, 2008.

[5] A. Zakariazadeh, S. Jadid, and P. Siano, “Smart microgrid energy and reserve scheduling with demand response using stochastic optimization,” International Journal of Electrical Power & Energy Systems., vol. 63, pp. 523-533, 2014.

[6] A. Zakariazadeh, S. Jadid, and P. Siano, “Economic-environmental energy and reserve scheduling of smart distribution systems: A multi objective mathematical programming approach,” Energy Convers. Manag. , vol. 78, pp. 151–164, 2014.

[7] Kia, Mohsen, et al. “An efficient linear model for optimal day ahead scheduling of CHP units in active distribution networks considering load commitment programs,” *Energy*, vol. 139, pp. 798-817, 2017.

[8] Li, Yang, et al. “Optimal scheduling of an isolated microgrid with battery storage considering load and renewable generation uncertainties,” IEEE Transactions on Industrial Electronics, vol. 66.2, pp. 1565-1575, 2018.

[9] B. Bahmani-Firouzi and R. Azizipanah-Abarghooee, “Optimal sizing of battery energy storage for micro-grid operation management using a new improved bat algorithm,” International Journal of Electrical Power & Energy Systems, vol. 56, pp. 42-54, 2014.

[10] A. Dolatabadi and B. Mohammadi-Ivatloo. “Stochastic risk-constrained scheduling of smart energy hub in the presence of wind power and demand response,” Applied Thermal Engineering, vol. 123, pp. 40-49, 2017.

[11] C. M. Correa-Posada, and P. Sánchez-Martin, “Security-constrained optimal power and natural-gas flow,” IEEE Trans. on Power Syst., vol. 29, no. 4, pp. 1780–1787, 2014.

[12] C. Liu, M. Shahidehpour, Y. Fu, and Z. Li, “Security-constrained unit commitment with natural gas transmission constraints,” IEEE Trans. Power Syst., vol. 24, no. 3, pp. 1523–1536, 2009.

[13] X. Zhang, L. Che, M. Shahidehpour, A. Alabdulwahab and A. Abusorrah, “Electricity-Natural Gas Operation Planning With Hourly Demand Response for Deployment of Flexible Ramp,” IEEE Transactions on Sustainable Energy, vol. 7, no. 3, pp. 996-1004, 2016.

[14] M. Geidl and G. Andersson. “Optimal power flow of multiple energy carriers,” IEEE Transactions on Power Systems, vol. 22, no. 1, pp. 145-155, 2007.

[15] S. Manshadi and M. Khodayar, “Resilient operation of multiple energy carrier microgrids,” IEEE Trans. Smart Grid, vol. 6, no. 5, pp. 2283–2292, 2015.

[16] Ramírez-Elizondo, Laura M., and GC Bob Paap. “Scheduling and control framework for distribution-level systems containing multiple energy carrier systems: Theoretical approach and illustrative example,” International Journal of Electrical Power & Energy Systems, vol. 66, pp. 194-215, 2015.

[17] MH Shams, Majid Shahabi, and Mohammad E. Khodayar. “Stochastic day-ahead scheduling of multiple energy Carrier microgrids with demand response,” Energy, vol. 155, pp. 326-338, 2018.

[18] MH Shams, Majid Shahabi, and Mohammad E. Khodayar. “Risk-averse optimal operation of Multiple-Energy Carrier systems considering network constraints,” Electric Power Systems Research, vol. 164, pp. 1-10, 2018.

[19] G. Boyle, Renewable energy, Oxford, U.K.: Oxford Univ. Press, 2004.

[20] J. Zeng, J. F. Liu, J. Wu and H. W. Ngan, “A multi-agent solution to energy management in hybrid renewable energy generation system,” Renewable Energy, vol. 36, no. 5, pp. 1352-1362, 2011

[21] D. Q. Hung, N. Mithulananthan and K. Y. Lee, “Determining PV Penetration for Distribution Systems With Time-Varying Load Models,” IEEE Trans. on Power Systems, vol. 29, no. 6, pp. 3048-3057, 2014.

[22] A. Safdarian, M. Fotuhi-Firuzabad and M. Lehtonen, “Integration of Price-Based Demand Response in DisCos' Short-Term Decision Model,” IEEE Transactions on Smart Grid, vol. 5, no. 5, pp. 2235-2245, 2014.

[23] E. S. Menon, Gas Pipeline Hydraulics. New York: Taylor & Francis, 2005.

[24] GAMS/SCENRED Documentation. Online: www.gams.com/docs/document.htm.

[25] CPLEX manual – GAMS. Online: www.gams.com/dd/docs/solvers/cplex.pdf.